Chemistry Europe
European Chemical Societies Publishing

WILEY VCH

Excellence in Chemistry Research

Announcing our new flagship journal

- Gold Open Access
- Publishing charges waived
- Preprints welcome
- Edited by active scientists

Meet the Editors of *ChemistryEurope*

Luisa De Cola
Università degli Studi di Milano Statale, Italy

Ive Hermans
University of Wisconsin-Madison, USA

Ken Tanaka
Tokyo Institute of Technology, Japan

Chemistry–A European Journal
Research Article
doi.org/10.1002/chem.202301438
Chemistry Europe
European Chemical Societies Publishing
www.chemeurj.org

Mixed-Valence Tetrametallic Iridium Chains

M. Pilar del Río,[a] B. Eva Villarroya,[a] José A. López,[a] Ana M. Geer,[a] Fernando J. Lahoz,[a] Miguel A. Ciriano,*[a] and Cristina Tejel*[a]

Neutral [X–{Ir_2}–{Ir_2}–X] (X=Cl, Br, SCN, I) and dicationic [L–{Ir_2}–{Ir_2}–L]$^{2+}$ (L = MeCN, Me_2CO) tetrametallic iridium chains made by connecting two dinuclear {Ir_2} units ({Ir_2} = [Ir_2(μ-OPy)$_2$(CO)$_4$], OPy = 2-pyridonate) by an iridium–iridium bond are described. The complexes exhibit fractional averaged oxidation states of +1.5 and electronic delocalization along the metallic chain. While the axial ligands do not significantly affect the metal–metal bond lengths, the metallic chain has a significant impact on the iridium–L/X bond distances. The complexes show free rotation around the unsupported iridium-iridium bond in solution, with a low-energy transition state for the chloride chain. The absorption spectra of these complexes show characteristic bands at 438–504 nm, which can be fine-tuned by varying the terminal capping ligands.

Introduction

Recent years have witnessed a growing interest in the synthesis of discrete chains of metal atoms due to their unique structures and interesting photophysical, magnetic, and redox properties.[1] Furthermore, their one-dimensional configuration makes them suitable for studying quantum transport across molecular junctions.[2] Also interesting is their potential applications as nanoscale devices such as wires or switches,[3] single molecular magnets,[4] and luminescent materials.[5] Moreover, these metallic chains are expected to undergo multi-electron transfer processes, which could facilitate small molecule activation.[6]

Nevertheless, this interest contrasts with the slow development of the field mainly due to the scarcity of reproducible synthetic methods.[1a] In this regard, a popular approach concerns the use of rationally designed multi-donor ligands as templates to linearly orient metal atoms. Such is the case of oligo-α-pyridyl/naphthyridyl amido[7] and related ligands,[8] which have been successfully used to host metal atoms in a linear array from three to the remarkable undecanickel string; the longest extended metal atom chain (EMAC) reported up to date.[9] Moreover, heteronuclear metal string complexes,[10] metal-defective strings,[11] and more complicated structures having multiply bonded dimetal units,[12] and mixed-valence cores[13] have also been prepared with this type of multidentate ligands.

In addition, low-valent metal atom chains of palladium and platinum atoms have been prepared with P-based ligands such as methylene-bridged tri-, tetra-, and hexa-phosphines.[14] Moreover, mixed PNNP- and PCP-type ligands have been used to stabilize metallic chains of copper, silver and gold.[15]

π-conjugated polyenes have also been described as suitable scaffolds to accommodate palladium ions in linear arrays,[16] which show efficient delocalization of the positive charge over the polyene ligands.[17] Among them, the decanuclear homo- and heterometallic chains sandwiched by two β-carotene ligands are remarkable.[18] Additionally, these scaffolds have allowed for the observation of interesting processes such as metal-translocation[19] and oxidative deprotonation of the ligand.[20]

Whereas with this **'ligand-assisted'** methodology, the number of metal atoms hosted in the chain is limited to the number of donor atoms (or C=C bonds) in the ligand, a second alternative, the '**metal-assisted**' approach, is based on growing the chain through the formation of unsupported metal–metal interactions or bonds. The main advantage of this methodology is that there are no limitations to the chain length other than the thermodynamic stability of the compound, although it requires keeping at a minimum the steric encumbrance between the links. In this context, metal···metal interactions between the metals placed at the end positions of preformed linear chains have allowed the preparation of octanuclear species with [{Pd_4}···{Pd_4}][21] and [{Au_4}···{Au_4}] cores.[22] Interestingly, some of them catalyze electrochemical hydrogen formation.[23] In addition, a remarkable decanuclear heterometallic chain displaying Au^{I}···Pb^{II} interactions has been recently reported.[24]

Closely related, bi- and tri-nuclear complexes have been connected by metal···metal interactions based on HOMO–LUMO interactions at the d_z^2 orbitals between platinum and heterometal atoms such as rhodium and ruthenium.[25] In general terms, the σ* HOMO is provided by platinum(II) complexes, whereas the σ* HOMO comes from paddlewheel rhodium(II) or ruthenium(II) compounds. Recent examples include hexametallic chains with [{Pt_2}···{Rh_2}···{Pt_2}], [{Rh_2}···{Pt_2}···{Rh_2}], and

[a] Dr. M. Pilar del Río, Dr. B. E. Villarroya, Dr. J. A. López, Dr. A. M. Geer, Prof. Dr. F. J. Lahoz, Prof. Dr. M. A. Ciriano, Dr. C. Tejel
Departamento de Química Inorgánica
Instituto de Síntesis Química y Catálisis Homogénea (ISQCH)
CSIC-Universidad de Zaragoza
Pedro Cerbuna 12, Facultad de Ciencias, 50009 Zaragoza (Spain)
E-mail: mciriano@unizar.es
ctejel@unizar.es

Supporting information for this article is available on the WWW under https://doi.org/10.1002/chem.202301438

[{PtMPt}···{PtMPt}] (M=Mn, Fe, Co, Ni, Cu) cores,[26] as well as mono-dimensional chains.[27]

Connecting the preformed links by unsupported covalent metal–metal bonds generally leads to more robust metallic chains. Such is the case of mixed-valent rhodium, iridium and platinum '*blues*'.[28] These species feature dinuclear complexes connected by unsupported metal–metal bonds, fractional averaged oxidation states of the metals and electronic delocalization along the metallic chain. Whereas a wide range of platinum '*blues*' and related complexes have been already described,[29] little is known on their Group 9 congeners, for which very few examples of tetranuclear ([{M_2}–{M_2}], M = Rh, Ir),[30] along with a sole example for hexanuclear ([{Ir_2}–{Ir_2}–{Ir_2}])[31] chains have been reported.

For both type of metal-strings, i.e., those in which the metal ions are linearly placed via coordination to multidentate ligands and those in which preformed links are connected by covalent or non-covalent unsupported metal-metal bonds, the influence of the capping ligands placed at the end of the chains on the structural, electronic, photo-physical, and magnetic properties is remarkable. For example, in the case of the most studied trinuclear EMACs, featuring [X–{M_3}–X] cores, it has been demonstrated that the identity of these ligands (X) significantly affects the metal···metal separations, the antiferromagnetic coupling parameter,[32] and the luminescence[33] (M=Ni), the symmetrical (Cr–Cr–Cr) versus unsymmetrical (Cr≡Cr···Cr) structures,[34] the spin-crossover properties (M=Co),[35] the color in mixed-valent trinuclear platinum chains,[36] as well as the metal–metal bond order and electric conductance (M=Ru).[37] Moreover, the spin-state of Co[7c] and Ni[8a] ions in [X–Cr_2Co–X] and [$Ni_3(NCS)_{2/1}]^{0/+1}$ systems, respectively, can be tuned by the π-donor/acceptor properties of the axial ligands. In addition, remoted effects of the axial ligands bonded to chromium on the structure of the metal M have been also observed in hetero-trimetallic chains [X'–Cr_2M–X] (M = Fe, Mn, Co).[38] Furthermore, the structures and electronic states of tetrametallic [L–{Pd_4}–L][14b] and octametallic [L–{Pd_4}···{Pd_4}–L][21a] chains have found to be controlled by the nature of the terminal capping ligands.

In the present study, we have explored the influence of the axially capped terminal ligands (L, X) on the structural and electronic properties of tetranuclear iridium '*blues*' featuring both, dicationic [L–{Ir_2}–{Ir_2}–L]$^{2+}$ (L = NCMe, Me_2CO) and neutral [X–{Ir_2}–{Ir_2}–X] (X = halide, *pseudo*halide) moieties.

Results and Discussion

Synthesis of the complexes. We previously communicated[30a] the easy one-electron oxidation of the dinuclear complex [Ir_2(μ-OPy)$_2$(CO)$_4$] (**1**) (OPy = 2-pyridonate) with [$FeCp_2$]PF_6 in acetonitrile to give the tetranuclear iridium '*blue*' [MeCN–{Ir_2}–{Ir_2}–NCMe]$(PF_6)_2$ ([**2**]$(PF_6)_2$, {Ir_2} = [Ir_2(μ-OPy)$_2$(CO)$_4$]), in which the metals show an average oxidation state of +1.5. The labile character of both capping acetonitrile ligands makes them suitable for easy exchange reactions. Thus, the simple solution of [MeCN–{Ir_2}–{Ir_2}–NCMe]$(PF_6)_2$ ([**2**]$(PF_6)_2$) in acetone causes an easy ligand replacement reaction of acetonitrile by acetone to give [Me_2CO–{Ir_2}–{Ir_2}–$OCMe_2$]$(PF_6)_2$ ([**3**]$(PF_6)_2$). In the same line, addition of LiCl, KBr, KI, and KSCN to acetone solutions of [**3**]$(PF_6)_2$ produced the incorporation of the halide/*pseudo*halide to both ends of the chain to form the neutral counterparts [X–{Ir_2}–{Ir_2}–X] (X = Cl, **4**; Br, **5**; I, **6**, NCS, **7**, Scheme 1). From these solutions the complexes were isolated as microcrystalline solids in very good yields. Complex **6** can be alternatively prepared by direct oxidation of [Ir_2(μ-OPy)$_2$(CO)$_4$] with iodine.[30b]

Unfortunately, all attempts to coordinate CN^- and OH^- anions to the ends of the chains were unsuccessful, leading to a mixture of unidentified complexes.

Molecular structures. Single crystals suitable for X-ray diffraction analyses of the iridium '*blues*' [**3**]$(PF_6)_2$, **4**, **5** and **7** were obtained by slow diffusion of hexane into acetone or dichloromethane solutions of the complexes. The molecular structures are displayed in Figure 1. Complexes [**3**]$(PF_6)_2$, **4**, and **7** crystallized in centrosymmetric groups, whereas **5** crystallized in the non-centrosymmetric group P 2_1.

All of them show a tetrairidium chain achieved through an unsupported iridium–iridium bond between two dinuclear [Ir_2(μ-OPy)$_2$(CO)$_4$] moieties, and two supported iridium–iridium bonds within each one of the dinuclear entities. The dinuclear moieties display a *face*-to-*face* structure bridged by two 2-pyridonate ligands in a *head*-to-*head* disposition. This config-

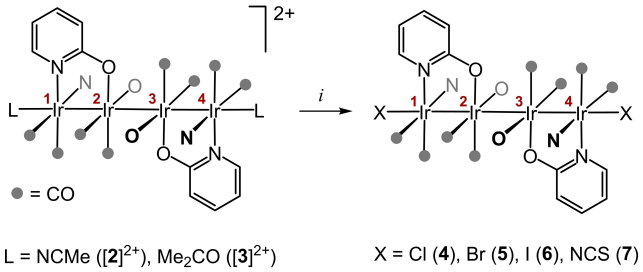

Scheme 1. Synthesis of neutral [X–{Ir_2}–{Ir_2}–X] chains (**4**-**7**) from $[\mathbf{3}]^{2+}$. *i* = LiCl, KBr, KI, and KSCN, respectively.

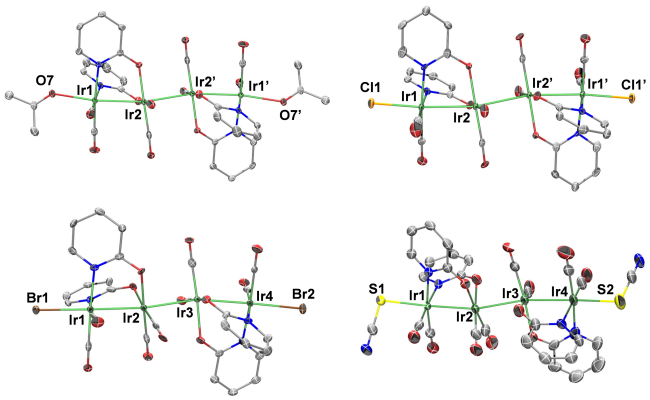

Figure 1. Molecular structures (ORTEP, ellipsoids set at 50% probability) of the cation of [**3**]$(PF_6)_2$ and the neutral iridium chains **4**, **5** and **7**. For the centrosymmetric complexes [**3**]$(PF_6)_2$ and **4** primed atoms are related with the unprimed ones by an inversion center. H-atoms have been omitted for clarity.

Table 1. Selected crystallographic and DFT-calculated (in italic) bond distances (Å) and angles (°) for tetranuclear iridium '*blues*'.[a]

Complex	L/X–Ir1 L/X–Ir4	Ir–Ir supp	Ir–Ir unsupp	θ	φ
$[\mathbf{2}]^{2+}$ (NCMe)	2.246(10)	2.6966(8) *2.741*	2.7772(10) *2.758*	168.03(3)	0 *−35.8*
$[\mathbf{3}]^{2+}$ (OCMe2)	2.378(2)	2.6836(2) *2.743*	2.7339(3) *2.751*	166.47(1)	0 *−34.9*
4 (Cl)	2.520(2)	2.7106(4) *2.741*	2.7840(5) *2.778*	167.41(2)	0 *−39.1*
5 (Br)	2.6833(14)	2.6917(7) *2.745*	2.7650(7) *2.785*	168.85(2)	−30.57(2) *−32.5*
6 (I)	2.843(2)	2.7015(15) *2.745*	2.750(2) *2.777*	168.20(5)	40.08(5) *−38.8*
7 (SCN)	2.563(3)	2.6934(5) *2.748*	2.7471(5) *2.787*	167.36(2)	−34.88(2) *−33.1*

[a] Supported (sup.) Ir–Ir bond = Ir1–Ir2, Ir3–Ir4; unsupported (unsupp.) Ir–Ir bond = Ir2–Ir2′/Ir3; θ = averaged value between θ1 and θ2 (θ1 = Ir1–Ir2–Ir2′/Ir3, θ2 = Ir2–Ir3–Ir4); φ = torsional twist angle around the unsupported Ir–Ir bond, calculated as the averaged value of the four O–Ir–Ir–C dihedral angles, see Figure 2 for details. Averaged values have been included for the non-centrosymmetric complexes **5** and **7**.

uration lead to two different types of iridium centers, *O,O*- and *N,N*-coordinated, and the unsupported metal–metal bond is formed between the *O,O*-coordinated iridium atoms, that is, the less hindered centers. Two solvent molecules ($OCMe_2$, $[\mathbf{3}]^{2+}$), halide (Cl, **4**; Br, **5**) or *pseudo*-halide (SCN, **7**) axial ligands are placed at both ends of the chains. The thiocyanide ligand was found to be *S*-coordinated in **7**, in contrast with the typical *N*-coordination observed in EMACs of first row transition metals.

Selected bond distances (Å) and angles (°) have been collected in Table 1, which also includes the structural data of the acetonitrile[30a] and iodide tetranuclear counterparts[30b] for comparative purposes.

In all the cases, the four iridium centers are arranged in a slightly zigzag chain, as deduced from the θ angles, calculated as the averaged value between θ1 (Ir1–Ir2–Ir2′/Ir3) and θ2 (Ir2–Ir3–Ir4) angles.

A particular feature refers to the relative conformation of the dinuclear entities around the unsupported metal–metal bond. They were found to be almost fully eclipsed in complexes $[\mathbf{2}]^{2+}$, $[\mathbf{3}]^{2+}$, and **4**, but alternated in *ca.* 35° for **5**–**7**, according to the torsional twist angle φ (calculated as the average of the four dihedral angles O–Ir–Ir–C around the unsupported Ir–Ir bond, Figure 2, Table 1). We don't find any electronic/steric reason to account for this difference, which probably arises from packing effects, and also because the very small energy difference between these conformations in the gas phase (see below).

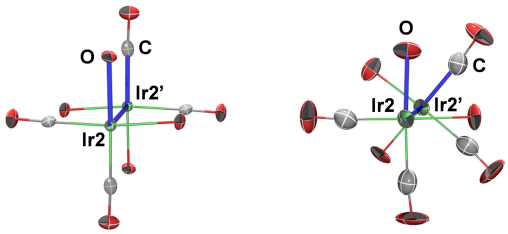

Figure 2. Central core of complexes [X–{Ir_2}–{Ir_2}–X] (X=Cl (**4**), on the left; I (**6**) on the right) showing the eclipsed and alternated cores, respectively, and one of the four diedral angles around the unsupported Ir–Ir bond (O–Ir–Ir–C) in blue.

The influence exerted by the axial ligand on both the supported (Ir1–Ir2, Ir3–Ir4) and unsupported (Ir2–Ir2′/Ir3) metal–metal bonds was found to be very small, although slightly marked for the later (Table 1). In the particular case of the eclipsed complexes (φ = 0; $[\mathbf{2}]^{2+}$, $[\mathbf{3}]^{2+}$, and **4**) both metal–metal bond distances increase simultaneously, following the sequence $OCMe_2 < NCMe < Cl$. For the alternated chains (**5**–**7**) no appreciable changes were observed on the supported metal–metal bond distances, despite of the different electronic properties of the axial ligand.

Conversely, the influence exerted by the metallic chain on the iridium–L/X bond distance was found to be remarkable considering the weak coordination of the axially bonded capping ligands. Thus, the Ir–$OCMe_2$ bond distance in the acetone chain $[\mathbf{3}]^{2+}$ is the longest reported up to date, being longer than that found in the mononuclear complex $[Ir(PCy_3)_2(H)_2(\eta\text{-}OCMe_2)_2]^+$, in which the *trans* influence of the terminal hydride ligand produces an elongation of the Ir–O bond up to 2.2379(13) Å.[39] A similar labile coordination of acetonitrile to iridium was found in $[\mathbf{2}]^{2+}$, for which the sole example of a longer Ir–NCMe bond distance was found in the acetonitrile *trans* to a nitrosyl ligand in $[Ir(NCMe)_3(NO)(PPh_3)_2]^{2+}$ (2.360(26) Å).[40] In addition, for complexes featuring the 'MeCN–Ir–Ir' moiety, the longest Ir–NCMe bond distance reported up to date was found shorter than here ($[Ir_2(\mu\text{-}ArNCNAr)_2(NCMe)_6]^{2+}$, 2.209(5) Å).[41]

In the same line, the halide chains, **4**, **5** and **6**, also feature relatively long Ir–X bond distances. A search on Cambridge Structural Database (CSD)[42] revealed very few examples of complexes with 'X–Ir–Ir' moieties showing longer Ir–X bond distances than here (X=Cl,[43] Br,[44] I[45]). This feature is even more pronounced for the thiocyanate derivative **7**, in which the coordination of the thiocyanate is weakly produced through the sulfur atom, as evidenced from the extremely long Ir–S bond distances (Table 1).[46]

DFT studies. Further insight into the ground state electronic structures of the iridium '*blues*' was gathered from DFT single point calculations, which were performed with B3LYP–D3 functional and LanL2TZ(f) (for Ir) and 6-311G(d,p) (for others) basis sets. In all the cases, the more stable conformer was found to be the alternated one, as found for complexes **5**, **6** and **7** in the solid state. For this particular conformation, the unsupported iridium–iridium bond length in the cationic complexes was found to be shorter than in the neutral ones, whereas no appreciable changes were observed on the supported iridium–iridium bond distances (Table 1).

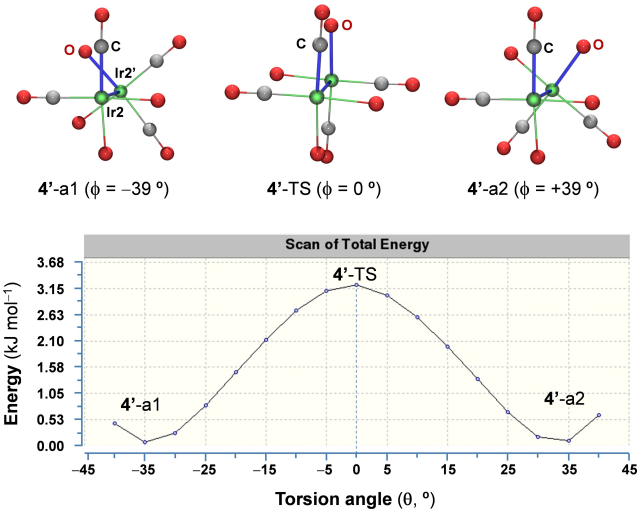

Figure 3. Central core of DFT-calculated **4'**-a1, **TS**, and **4'**-a2 (top) and scan of total energy for the rotation of one of the dinuclear entities around the unsupported metal–metal bond. φ = torsional twist angle around the unsupported Ir–Ir bond, calculated as the averaged value of the four O–Ir–Ir–C dihedral angles, see Figure 2 for details.

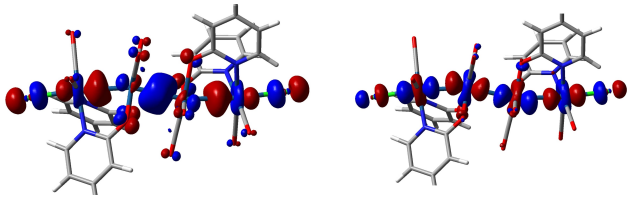

Figure 4. HOMO (left) and LUMO (right) of the tetrametallic chain [Cl–{Ir_2}–{Ir_2}–Cl] (**4**).

In the particular case of the chloride chain **4**, the rotation of one of the dinuclear entities around the unsupported metal–metal bond was analyzed by DFT calculations. As shown in Figure 3, two minima were located for the alternated conformations **4'**-a1 and **4'**-a2, which featured values of φ = −39.05 and +39.05°, respectively, and similar Δ*E* values.

To our surprise, the eclipsed conformation (φ = 0°), found in the solid state, corresponds to the transition state (**4'**-TS) between the two alternated ones. This **4'**-TS was found to be 3.6 kJ mol^{-1} above the two symmetrical more stable alternated conformations (**4'**-a1 and **4'**-a2), indicating that such a rotation is a very low energy process. Moreover, the unexpected crystallization of **4'**-TS clearly indicates the influence of packing effects in stabilizing a particular conformation.

In all the cases the HOMO's and LUMO's are both mainly metal-centered molecular orbitals corresponding to two of the four combinations of the iridium d_z^2 orbitals. The HOMO's (σ*,σ,σ*) show a bonding character for the inter–dimer σ-Ir2–Ir2'/Ir3 bond and antibonding nature for the intra–dimer metal–metal bonds whereas the LUMO's develop an antibonding character between every pair of adjacent iridium atoms (σ*,σ*,σ*) (Figure 4).

The electron vacancy of these high-energy σ-MO's is the responsible for the stability of the unsupported metal–metal bond between the two dinuclear moieties. Moreover, the stability of the metal chain is assigned to a 2-electron/4-center delocalized σ-bond along the metal backbone.

The HOMO–LUMO gaps varies from 3.208 to 2.822 eV, found for the acetonitrile ($[\mathbf{2}]^{2+}$) and the iodide (**6**) chains, respectively (Table 2a). Under the perspective that larger HOMO–LUMO

Table 2. a) Selected electronic DFT parameters for tetranuclear iridium '*blues*'.[a] b) Wiberg bond indices (WBI).[b]

Complex	$[\mathbf{3}]^2$ ($OCMe_2$)	$[\mathbf{2}]^{2+}$ (NCMe)	**4** (Cl)	**5** (Br)	**7** (SCN)	**6** (I)
a)						
ΔE	3.015	**3.208**	3.029	2.948	2.854	**2.822**
Ir(int)$^{\delta-}$	−0.173	−0.188	−0.241	−0.230	−0.237	−0.234
Ir(ext)$^{\delta-}$	**−0.247**	**−0.327**	**−0.429**	**−0.475**	**−0.507**	**−0.740**
χ (AR)	3.50	3.07	2.83	2.74	2.44	2.21
b)						
Ir–Ir supp	0.4662	0.4725	0.4712	0.4628	0.4553	0.4359
Ir–Ir unsup	0.5070	0.4992	0.4570	0.4535	0.4508	0.4493
Ir(ext)–L/X	0.2495	0.3761	0.6153	0.6360	0.5973	0.9041

[a] Ir(int) = internal iridium, Ir(ext) = external iridium. For complexes **5** and **7**, averaged values of the electronic density on internal Ir2 and Ir3 and external Ir1 and Ir4 (ext) are shown, χ = Allred-Rochow electronegativity of the heteroatom bonded to iridium in the capping ligand, ΔE (HOMO–LUMO) in ev. [b] For non symmetric complexes, Ir–Ir(supp) corresponds to the averaged value of WBI for Ir1–Ir2 and Ir3–Ir4 bons. In the case of Ir(ext)–L/X, averaged values have been also included.

gaps correspond to better stability, the acetonitrile complex is expected to be the more stable tetrametallic chain.

NBO analyses were utilized to estimate the natural charge population on the iridium atoms. According to Table 2a, the partial negative charge on the iridium atoms located at the end of the chains (Ir(ext)) is seen to increase as the electronegativity (Allred-Rochow scale) of the heteroatom in the capping ligand decreases.

The Wiberg bond indices (WBI) indicate the existence of three metal–metal bonding interactions within the tetrametallic chains (Table 2b). The values for the supported and unsupported Ir–Ir bonds were observed to be alike, which agree with a complete delocalization of the two electrons along the chain. Moreover, the bonding between the axial ligand and the external iridium atoms was found to be strong for iodide, whereas it appeared to be weak for the acetonitrile and acetone ligands.

NMR studies. The isolated chains show a relative stability in solution, giving the expected resonances in the ^{1}H and $^{13}C\{^{1}H\}$ NMR spectra. Free rotation around the unsupported iridium–iridium bond in solution makes equivalent the four 2-pyridonate ligands, leading thus to four resonances in their ^{1}H NMR spectra. It is worth noting the influence of the axial ligand in the chemical shift of the proton H^{6} when comparing their ^{1}H NMR spectra in CD_2Cl_2 solutions (Figure 5).

At first glance, a hydrogen bond interaction between the H^{6} proton and the axial heteroatom bonded to iridium (typically at ≈2.6 Å) could be the responsible of these shifts, exerting a stronger influence the more electronegative heteroatom. However, the most deshielded proton was found to be that in the iodo complex **6**, ruling out this possibility.

A second alternative that better accounts for the observed chemical shifts is related to the strength of the Ir–X bond. Under this perspective, complexes $[\mathbf{2}]^{2+}$, $[\mathbf{3}]^{2+}$, and **7**, which feature weakly coordinated acetonitrile, acetone, and thiocyanate ligands (Table 1), shows the more shielded H^{6} protons, whereas they are high field shifted for the halide series. For them, the observed trend Cl < Br < I matches well with the expected increase of the Ir–X bond strength (Cl < Br < I).[47] Noticeably, this trend was also observed in their corresponding $^{13}C\{^{1}H\}$ NMR spectra, where again the more deshielded C^{6} carbon was found in the iodide complex **7** (see the Supporting Information).

UV-Vis studies. The tetranuclear iridium '*blues*' are distinguished by their intense coloration, both in solid state and in solution, which is indicative of electronic transitions in the visible spectrum. These transitions are directly related to the difference in energy between the chain's orbitals and may provide additional information about the influence of the axial ligands on the electronic structure.

To prevent the exchange of the axial ligands by solvent molecules, samples of $[\mathbf{2}](PF_6)_2$ and $[\mathbf{3}](PF_6)_2$ were prepared in acetonitrile and acetone respectively, whereas the neutral chains **4**–**7** were dissolved in dichloromethane. Figure 6 shows the UV/Vis spectra in solution of the aforementioned compounds. Additionally, Table 3 collects the data of wavelength and molar extinction coefficients, along with those calculated values from TD-DFT calculations.

All the complexes gave a very intense absorption band in the visible region with molar extinction coefficients ranging $3.3\cdot10^{4}$–$9.6\cdot10^{4}$ L mol^{-1} cm^{-1} (allowed transitions by the selection rules). The lower values of wavelength were obtained for the cationic chains $[\mathbf{2}](PF_6)_2$ and $[\mathbf{3}](PF_6)_2$ (438 and 455 nm, respectively), whereas the higher band was observed for the neutral iodide **6** (504 nm). An appreciable red shift was observed according to the sequence $[\mathbf{2}]^{2+} < \mathbf{4} < \mathbf{5} < \mathbf{7} < \mathbf{6}$, which nicely fits with a decrease in the electronegativity (Allred-Rochow scale) of the heteroatom in the axial capping ligand (Table 3). The sole exception to this general trend corresponds to the acetone complex ($[\mathbf{3}]^{2+}$), featuring the most electronegative atom (oxygen), probably due to the labile coordination of the acetone molecules to iridium above mentioned.

TD-DFT calculations reproduced considerably well the experimental electronic absorption spectra (Table 3). The estimated lowest energy singlet excited state (S1) was found to be placed from 2.81 to 2.49 eV (from 441.6 to 497.5 nm) above the ground state (S0) with very large oscillator strength (f) in all the cases. The calculated transitions are assignable to spin allowed

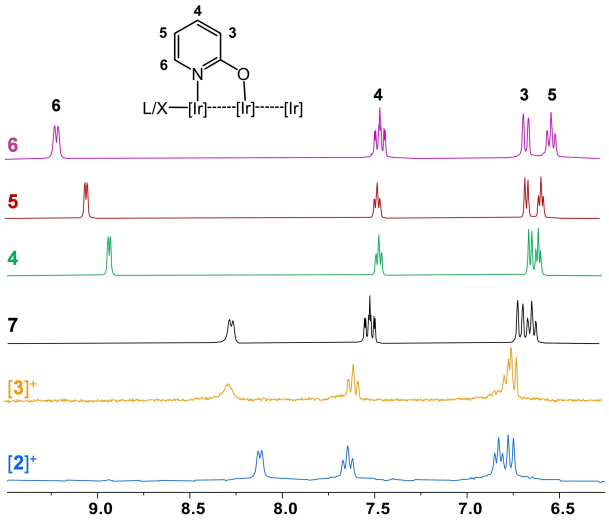

Figure 5. ^{1}H NMR spectra of complexes $[\mathbf{2}]^{2+}$, $[\mathbf{3}]^{2+}$, and **4**–**7** in CD_2Cl_2.

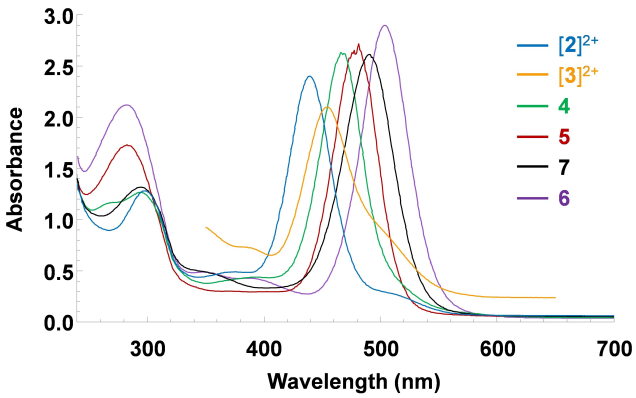

Figure 6. UV-Vis of complexes $[\mathbf{2}]^{2+}$ (in acetonitrile), $[\mathbf{3}]^{2+}$ (in acetone), and **4**–**7** in CH_2Cl_2.

Table 3. UV-vis spectra and selected TD-DFT data for tetranuclear iridium '*blues*'.[a]

Complex	$[\mathbf{3}]^{2+}$	$[\mathbf{2}]^{2+}$	**4**	**5**	**7**	**6**
L/X	Me_2CO	NCMe	Cl	Br	NCS	I
χ (AR)	3.50	3.07	2.83	2.74	2.44	2.21
λ (nm)	455	438	467	481	490	504
ε	3.3·104	5.4·104	6.0·104	9.1·104	8.4·104	9.6·104
Δ(S0–S1)	2.67	2.81	2.70	2.61	2.51	2.49
λ (nm)	464.4	441.6	458.5	475.3	494.4	497.5
f	1.0171	0.8956	1.0913	1.2198	1.4010	1.5883
%	93%	90%	92%	95%	96%	97%

[a] Registered on solutions *ca.* 10^{-5} in acetonitrile ($[\mathbf{2}]^{2+}$), acetone ($[\mathbf{3}]^{2+}$), and dichloromethane (**4**–**7**);. ε in L mol^{-1} cm^{-1}, χ = Allred-Rochow electronegativity, Δ(S0–S1), f = oscillator strength, and % = % of HOMO to LUMO contribution (main transition).

HOMO to LUMO transitions (ca. 100%) and are in agreement with the observed absorption energies.

Conclusions

The impact of the axial capping ligand on the structural and electronic characteristics of a series of neutral and cationic tetranuclear iridium '*blues*' was explored. The complexes, of general formula [L–{Ir_2}–{Ir_2}–L]$^{2+}$ (L=MeCN, $[\mathbf{2}]^{2+}$; Me_2CO, $[\mathbf{3}]^{2+}$) and [X–{Ir_2}–{Ir_2}–X] (X = Cl, **4**; Br, **5**; I, **6**; SCN, **7**), consist of two dinuclear {Ir_2} units ({Ir_2}=[$Ir_2(\mu\text{-}OPy)_2(CO)_4$], OPy = 2-pyridonate) linked by an unsupported iridium–iridium bond. A fractional averaged oxidation state of +1.5 and complete electron delocalization along the metallic chain was found in all the cases. This electron delocalization corresponds to a 2-electron/4-center delocalized π-bond along the metal backbone, and accordingly, the Wiberg bond indices (WBI) for the supported and unsupported by bridging ligands iridium–iridium bonds were almost identical in all the complexes.

Structural analyses indicate that the axial ligands do not have a significant impact on the metal–metal bond lengths. Conversely, the metallic chain strongly influences the distances between iridium and L/X atoms, with acetonitrile and acetone showing weak coordination, and iodide exhibiting a stronger Ir–X bond according to the WBI values.

The tetrametallic metal backbone is stable enough to be maintained in solution, where free rotation around the unsupported iridium–iridium bond was observed. In the particular case of the chloride chain, this rotation was estimated by DFT-calculations. Going from alternated un-clockwise conformation (φ = −39.05°) to the clockwise one (φ = 39.05°), a transition state corresponding to the eclipsed conformation (φ = 0°) was located only 3.6 kcal mol^{-1} above the alternated conformations. Noticeably, this transition state corresponds to the structure found in the solid state; enlighten the strong influence of packing effects in stabilizing a specific structure.

NMR studies showed a strong influence of the axial ligand in the chemical shift of the proton H^6 (and C^6), with the iodide complex showing the most deshielding effect. For the halide series, the observed trend Cl < Br < I matches well with the expected increase of the Ir–X bond strength (Cl < Br < I).

Finally, all the complexes gave a very intense absorption band in the visible region. An appreciable red shift was observed according to the sequence $[\mathbf{2}]^{2+} < \mathbf{4} < \mathbf{5} < \mathbf{7} < \mathbf{6}$, which is consistent with a decrease in the electronegativity (Allred-Rochow scale) of the heteroatom in the axial capping ligand.

Experimental Section

All the operations were carried out under an argon atmosphere using standard Schlenk techniques as well as dry-box facilities. Acetone was distilled from calcium hydride under argon and ultrapure acetonitrile was used as purchased from Aldrich. The other solvents were purified with a Solvent Purification System (MB-SPS-800). 2-hydroxypyridine (97%, Aldrich) and all other chemicals were purchased from commercial suppliers and used without further purification. Complex [MeCN–{Ir_2}–{Ir_2}–NCMe]$(PF_6)_2$ ($[\mathbf{2}](PF_6)_2$) was prepared according to literature methods.[30a] Carbon, hydrogen, and nitrogen analysis were carried out with Perkin–Elmer 2400 CHNS/O microanalyzer. NMR spectra were recorded on Bruker AV-400 and AV-500 spectrometers operating at 400.13 and 500.13 MHz respectively, for ^1H. Chemical shifts are reported in ppm and referenced to $SiMe_4$, using the internal signal of deuterated solvent as the reference (^1H and ^{13}C). IR spectra of solid samples were recorded with a Perkin–Elmer 100 FTIR spectrometer (4000–400 cm^{-1}) equipped with attenuated total reflectance (ATR). Electronic spectra were recorded on a double-beam UV-visible UNICAM UV-4 spectrophotometer., using a quartz cuvette sealed with an airtight Teflon® cap (optical path length l = 0.1 cm).

Synthesis of the complexes. [Me_2CO–{Ir_2}–{Ir_2}–$OCMe_2$]$(PF_6)_2$ ([3]$(PF_6)_2$): Complex $[\mathbf{2}](PF_6)_2$ (75.0 mg, 0.0431 mmol) was dissolved in 3 mL of acetone and layered with 6 mL of diethyl ether. After three days, the mother-liquid was decanted and the resulting green-turquoise crystals were washed with diethyl ether (3×2 mL) and vacuum-dried. Yield: 65.7 mg (86%). ^1H NMR (500.13 MHz, [D_6]acetone, 25 °C): δ = 8.32 (dd, $^3J(H,H) = 6.5$ Hz, $^4J(H,H) = 1.9$ Hz, 4H; H^6), 7.78 (ddd, $^3J(H,H) = 8.7$ Hz, $^4J(H,H) = 6.9$ Hz, $^5J(H,H) = 1.9$ Hz, 4H; H^4), 6.89 (t, $^3J(H,H) = 6.9$ Hz, 4H; H^5), 6.85 (d, $^3J(H,H) = 8.7$ Hz, 4H; H^3); $^{13}C\{^1H\}$ NMR (125.0 MHz, [D_6]acetone, 25 °C): δ = 174.1 (C2), 163.8 and 162.2 (Ir–*C*O), 146.6 (C6), 142.9 (C4), 118.2 (C3), 116.5 (C5); IR (nujol): ν = 2118 (s), 2095 (w), 2068 (s), 2056 (sh) (C≡O), 1653 (s, Me_2CO), 1618 (s, OPy) cm^{-1}; UV-Vis ($3.6 \cdot 10^{-5}$ M): λ_{max}(acetone) = 455 nm ($\varepsilon = 3.3 \cdot 10^4$ L mol^{-1} cm^{-1}), elemental analyses calcd. (%) for

$C_{34}H_{28}N_4O_{14}Ir_4P_2F_{12}$ (1775.4): C 23.00, H 1.59, N 3.16; found: C 22.56, H 1.30, N 3.28.

[Cl–{Ir$_2$}–{Ir$_2$}–Cl] (4): LiCl·H_2O (5.2 mg, 0.086 mmol) was added to an acetone solution (5 mL) of [**2**]$(PF_6)_2$ (75.0 mg, 0.0431 mmol). After stirring for one hour the red solution was evaporated to dryness. The residue was solved in dichloromethane and filtered to give a red solution, which was concentrated to 3 mL and layered with 7 mL of hexane. The mother-liquid was decanted and the red microcrystals were washed with hexane (3×2 mL) and vacuum-dried. Yield: 55.2 mg (89%). ^{1}H NMR (500.13 MHz, CD_2Cl_2, 25 °C): δ = 8.93 (dd, ^3J(H,H) = 6.4 Hz, ^4J(H,H) = 1.3 Hz, 4H; H^6), 7.47 (ddd, ^3J(H,H) = 8.7 Hz, ^4J(H,H) = 6.8 Hz, ^5J(H,H) = 1.9 Hz, 4H; H^4), 6.64 (d, ^3J(H,H) = 8.5 Hz, 4H; H^3), 6.60 (td, ^3J(H,H) = 6.7, ^4J(H,H) = 1.9 Hz, 4H, H^5); ^{13}C{^{1}H} NMR (125.0 MHz, CD_2Cl_2, 25 °C): δ = 176.1 (C2), 166.8 and 163.8 (Ir–CO), 146.8 (C6), 140.6 (C4), 117.2 (C3), 114.4 (C5); IR (nujol): ν = 2091 (vs), 2066 (s), 2044 (vs), 2025 (m) (C≡O), 1614 (s, OPy) cm^{-1}; UV-Vis ($5.7\cdot10^{-5}$ M): λ_{max}(dichloromethane) = 467 nm (ε = $6.0\cdot10^4$ L mol^{-1} cm^{-1}), elemental analyses calcd. (%) for $C_{28}H_{16}N_4O_{12}Ir_4Cl_2$ (1440.2): C 23.35, H 1.12, N 3.89; found: C 23.18, H 1.09, N 3.80.

[Br–{Ir$_2$}–{Ir$_2$}–Br] (5) was prepared as above starting from [**2**]$(PF_6)_2$ (75.0 mg, 0.0431 mmol) and KBr (10.3 mg, 0.0861 mmol) and isolated as maroon microcrystals. Yield: 51.4 mg (78%). ^{1}H NMR (500.13 MHz, CD_2Cl_2, 25 °C): δ = 9.05 (dd, ^3J(H,H) = 6.4 Hz, ^4J(H,H) = 2.0 Hz, 4H; H^6), 7.46 (ddd, ^3J(H,H) = 8.6 Hz, ^3J(H,H) = 6.8 Hz, ^4J(H,H) = 1.9 Hz, 4H; H^4), 6.65 (d, ^3J(H,H) = 8.6 Hz, 4H; H^3), 6.57 (td, ^3J(H,H) = 6.6 Hz, ^4J(H,H) = 1.4 Hz, 4H; H^5); ^{13}C{^{1}H} NMR (125.0 MHz, CD_2Cl_2, 25 °C): δ = 175.7 (C2), 166.6 and 164.1 (Ir–CO), 148.9 (C6), 140.5 (C4), 117.1 (C3), 114.7 (C5); IR (nujol): ν = 2089 (s), 2066 (s), 2044 (vs), 2025 (s) (C=O), 1616 (s, OPy) cm^{-1}; UV-Vis ($4.6\cdot10^{-5}$ M): λ_{max}-(dichloromethane) = 481 nm (ε = $9.1\cdot10^4$ L mol^{-1} cm^{-1}), elemental analyses calcd. (%) for $C_{28}H_{16}N_4O_{12}Ir_4Br_2$ (1529.1): C 21.99, H 1.05, N 3.66; found: C 21.87, H 1.06, N 3.61.

[I–{Ir$_2$}–{Ir$_2$}–I] (6) was prepared as above starting from [**2**]$(PF_6)_2$ (75.0 mg, 0.0431 mmol) and KI (14.3 mg, 0.0861 mmol) and isolated as purple microcrystals. Yield: 52.4 mg (75%). ^{1}H NMR (500.13 MHz, CD_2Cl_2, 25 °C): δ = 9.21 (dd, ^3J(H,H) = 6.4 Hz, ^4J(H,H) = 1.4 Hz, 4H; H^6), 7.45 (ddd, ^3J(H,H) = 8.7 Hz, ^4J(H,H) = 6.8 Hz, ^5J(H,H) = 1.9 Hz, 4H; H^4), 6.66 (ddd, ^3J(H,H) = 8.6 Hz, ^4J(H,H) = 1.4 Hz, ^5J(H,H) = 0.7 Hz, 4H; H^3), 6.52 (td, ^3J(H,H) = 6.7 Hz, ^4J(H,H) = 1.4 Hz, 4H; H^5); ^{13}C{^{1}H} NMR (125.0 MHz, CD_2Cl_2, 25 °C): δ = 175.3 (C2), 166.5 and 165.1 (Ir–CO), 152.9 (C6), 140.4 (C4), 117.1 (C3), 115.0 (C5); IR (nujol): ν = 2080 (s), 2069 (s), 2044 (vs), 2020 (s) (C=O), 1616 (s, OPy) cm^{-1}; UV-Vis ($2.6\cdot10^{-5}$ M): λ_{max}(dichloromethane) = 504 nm (ε = $9.6\cdot10^4$ L mol^{-1} cm^{-1}), elemental analyses calcd. (%) for $C_{28}H_{16}N_4O_{12}Ir_4I_2$ (1623.1): C 20.72, H 0.99, N 3.45; found: C 20.94, H 1.18, N 3.25.

[NCS–{Ir$_2$}–{Ir$_2$}–SCN] (7) was prepared as above starting from [**2**]$(PF_6)_2$ (75.0 mg, 0.0431 mmol) and KSCN (8.4 mg, 0.086 mmol) and isolated as orange microcrystals with metallic green brightness. Yield: 46.7 mg (73%). ^{1}H NMR (500.13 MHz, CD_2Cl_2, 25 °C): δ = 8.27 (br, 4H; H^6), 7.51 (ddd, ^3J(H,H) = 8.7 Hz, ^4J(H,H) = 6.8 Hz, ^5J(H,H) = 1.9 Hz, 4H; H^4), 6.69 (dd, ^3J(H,H) = 8.3 Hz, ^4J(H,H) = 1.3 Hz, 4H; H^3), 6.62 (td, ^3J(H,H) = 6.6 Hz, ^4J(H,H) = 1.4 Hz, 4H; H^5); ^{13}C{^{1}H} NMR (125.0 MHz, CD_2Cl_2, 25 °C): δ = 176.3 (C2), 166.1 and 163.4 (Ir–CO), 147.0 (C6), 140.9 (C4), 117.9 (C3), 115.4 (C5); IR (nujol): ν = 2109 (s, SCN), 2085 (s), 2066 (s), 2053 (s), 2025 (s), (C=O), 1617 (s, OPy) cm^{-1}; UV-Vis ($3.5\cdot10^{-5}$ M): λ_{max}(dichloromethane) = 490 nm (ε = $8.4\cdot10^4$ L mol^{-1} cm^{-1}), elemental analyses calcd. (%) for $C_{30}H_{16}N_6O_{12}Ir_4S_2$ (1485.5): C 24.26, H 1.09, N 5.66, S 4.32; found: found: C 24.24, H 1.14, N 5.46, S 4.35.

X-ray diffraction studies on complexes [Me_2CO–{Ir$_2$}–{Ir$_2$}–$OCMe_2$]$(PF_6)_2$ ([**3**]$(PF_6)_2$), [Cl–{Ir$_2$}–{Ir$_2$}–Cl] (4), [Br–{Ir$_2$}–{Ir$_2$}–Br] (5), and [NCS–{Ir$_2$}–{Ir$_2$}–SCN] (7): Intensity measurements were collected with a Bruker Smart Apex diffractometer with graphite-monochromated $Mo_{K\alpha}$ radiation at 100 K ([**3**]$(PF_6)_2$ and 5) or 130 K (4), except for (7), which was measured with BrukerAXS SMART APEXII CCD diffractometer installed at station 9.8 of the SRS Daresbury Laboratory, at 150 K. Synchrotron radiation was monochromated with a silicon (111) crystal (λ = 0.6934 Å). Data were collected with ω scans of 0.3°, and a semi-empirical absorption correction was applied to the data sets with the multi-scan[48] methods. The structures were solved by direct methods with SIR97[49] (7), SHELXS-97[50] ([**3**]$(PF_6)_2$ and 4) or SHELXS-2013[49] (5) and refined by full-matrix least-squares on F^2 with the program SHELXL-2016,[51] in the WINGX[52] package. All non-hydrogen atoms were refined with anisotropic displacement parameters, and their hydrogen atoms were geometrically calculated and refined by the riding mode, including the isotropic displacement parameters. In compound 7, the procedure SQUEEZE[53] was used to model a severe solvent disorder, accounting for six hexane molecules per unit cell. For selected crystallographic data see the Supporting Information.

Deposition Number(s) 2257856 ([**3**]$(PF_6)_2$), 2257855 (**4**), 2257858 (**5**·3CH_2Cl_2) and 2257857 (**7**·1.5 C_6H_{14}) contain(s) the supplementary crystallographic data for this paper. These data are provided free of charge by the joint Cambridge Crystallographic Data Centre and Fachinformationszentrum Karlsruhe Access Structures service.

DFT geometry optimizations: The DFT geometry optimizations were carried out with the Gaussian 09 program package,[54] using the B3LYP-D3 hybrid functional.[55] Geometry optimizations were performed in the gas phase with the LanL2TZ(f) effective core potential basis set for the metal atoms, and the 6-311G(d,p) basis set for the remaining ones. The LanL2TZ(f) basis set is based in the Hay–Wadt relativistic effective core potentials (RECPs) for the transition metal atoms.[56]

TD-DFT calculations: TD-DFT calculations were performed considering solvent effects of acetonitrile, acetone or dichloromethane with the continuum SMD model.[57]

Supporting Information

Selected crystallographic data, density functional theory orbitals, and ^{13}C{^{1}H} NMR spectra (pdf). Cartesian coordinates for optimized (DFT, TD-DFT) structures of the complexes (XYZ). Crystallographic data for complexes **3**]$(PF_6)_2$, **4**, **5**, and **7** (CIF). Additional references have not been cited within the Supporting Information.

Acknowledgements

The generous financial support from MCIN/AEI/10.13039/501100011033 (PID2020-119512GB-I00) and Gobierno de Aragon/FEDER, EU (GA/FEDER, Inorganic Molecular Architecture Group, E50_23R) is gratefully acknowledged. A.M.G. is thankful for Grant IJC2018-035231-I funded by MCIN/AEI/10.13039/501100011033. The 'Centro de Supercomputación de Galicia (CESGA)' is also gratefully acknowledged for generous allocation of time.

Conflict of Interests

The authors declare no conflict of interest.

Data Availability Statement

The data that support the findings of this study are available from the corresponding author upon reasonable request.

Keywords: metallic chains · iridium · mixed-valence · UV-vis · metal–metal bonds

[1] a) P. Braunstein, A. A. Danopoulos, *Chem. Rev.* **2021**, *121*, 7346–7397; b) Y. Tanaka, M. Kiguchi, M. Akita, *Chem. Eur. J.* **2017**, *23*, 4741–4749; c) J. F. Berry, in *Metal-metal bonds in chains of three or more metal atoms: from homometallic to heterometallic chains*, Vol 136 (Eds: G. Parkin.), Structure and Bonding, Springer, Berlin, Germany, **2010**, pp. 128; d) J. F. Berry, in *Multiple Bonds Between Metal Atoms*, 3rd Ed. (Eds: F. A. Cotton, C. A. Murillo, R. A. Walton), Springer, New York, **2005**, Ch. 15, pp. 669.

[2] G.-M. Lin, M.-C. Cheng, S.-J. Liou, H.-S. Tsao, C.-H. Lin, Y. R. Lin, G.-H. Lee, C.-h. Chen, S.-M. Peng, *J Chin Chem Soc.* **2019**, *66*, 1157–1164.

[3] a) Y. Kitagawa, H. Tada, I. Era, T. Fujii, K. Ikenaga, M. Nakano, *Molecules* **2019**, *24*, 1956; b) L.-Y. Hsu, B.-Y. Jin, C.-h. Chen, S.-M. Peng, *Chem* **2017**, *3*, 378–379; c) T.-C. Ting, L.-Y. Hsu, M.-J. Huang, E.-C. Horng, H.-C. Lu, C.-H. Hsu, C.-H. Jiang, B.-Y. Jin, S.-M. Peng, C.-h. Chen, *Angew. Chem.* **2015**, *127*, 15960–15964; *Angew. Chem. Int. Ed.* **2015**, *54*, 15734–15738; d) V. P. Georgiev, P. J. Mohan, D. DeBrincat, J. E. McGrady, *Coord. Chem. Rev.* **2013**, *257*, 290–298; e) D. DeBrincat, O. Keers, J. E. McGrady, *Chem. Commun.* **2013**, *49*, 9116–9118; f) I.-W. P. Chen, M.-D. Fu, W.-H. Tseng, J.-Y. Yu, S.-H. Wu, C.-J. Ku, C.-h. Chen, S.-M. Peng, *Angew. Chem.* **2006**, *118*, 5946–5950; *Angew. Chem. Int. Ed.* **2006**, *45*, 5814–5818; g) J. K. Bera, K. R. Dunbar, *Angew. Chem.* **2002**, *114*, 4633–4637; *Angew. Chem. Int. Ed.* **2002**, *41*, 4453–4457.

[4] a) A. Nicolini, M. Affronte, D. J. SantaLucia, M. Borsari, B. Cahier, M. Caleffi, A. Ranieri, J. F. Berry, A. Cornia, *Dalton Trans.* **2021**, *50*, 7571–7589; b) A. Srinivasan, R. A. Musgrave, M. Rouzières, R. Clérac, J. E. McGrady, E. A. Hillard, *Chem. Commun.* **2021**, *57*, 13357–13360; c) A. Cornia, A.-L. Barra, V. Bulicanu, R. Clérac, M. Cortijo, E. A. Hillard, R. Galavotti, A. Lunghi, A. Nicolini, M. Rouzières, L. Sorace, F. Totti, *Inorg. Chem.* **2020**, *59*, 1763–1777.

[5] a) T. P. Seifert, V. R. Naina, T. J. Feuerstein, N. D. Knöfel, P. W. Roesky, *Nanoscale* **2020**, *12*, 20065–20088; b) M. Stollenz, *Chem. Eur. J.* **2019**, *25*, 4274–4298 *and references therein*; c) P. Ai, M. Mauro, C. Gourlaouen, S. Carrara, L. De Cola, Y. Tobon, U. Giovanella, C. Botta, A. A. Danopoulos, P. Braunstein, *Inorg. Chem.* **2016**, *55*, 8527–8542.

[6] a) T. Tanase, Y. Morita, K. Sato, R. Aoki, A. Yoshii, K. Nakamae, Y. Ura, T. Nakajima, *J. Organomet. Chem.* **2021**, *939*, 121771; b) C. Tejel, S. Sancho, J. A. López, M. A. Ciriano, *Chem. Eur. J.* **2012**, *18*, 15250–15253.

[7] *See for example*: a) K. Aoki, K. Otsubo, Y. Yoshida, Y. Kimura, K. Sugimoto, H. Kitagawa, *Inorg. Chem.* **2021**, *60*, 16029–16034; b) P. Gao, X.-P. Cai, Q. Xie, Q. Yang, H. Ou, W.-Q. Wu, X. Xu, Z. Xu, X. Lin, *Inorg. Chem.* **2021**, *60*, 9378–9386; c) J. A. Chipman, J. F. Berry, *Chem. Rev.* **2020**, *120*, 2409–2447; d) B.-H. Wu, L.-Y. Hung, J.-Y. Chung, S.-M. Peng, I.-C. Chen, *J. Phys. Chem. C.* **2018**, *122*, 6332–6339; e) A. Nicolini, R. Galavotti, A.-L. Barra, M. Borsari, M. Caleffi, G. Luo, G. Novitchi, K. Park, A. Ranieri, L. Rigamonti, F. Roncaglia, C. Train, A. Cornia, *Inorg. Chem.* **2018**, *57*, 5438–5448; f) R. H. Ismayilov, W.-Z. Wang, G.-H. Lee, S.-M. Peng, B. A. Suleimanov, *Polyhedron* **2017**, *122*, 203–209; g) L.-H. Tsou, M. Sigrist, M.-H. Chiang, E.-C. Horng, C.-h. Chen, S.-L. Huang, G.-H. Lee, S.-M. Peng, *Dalton Trans.* **2016**, *45*, 17281–17289; h) L.-C. Yu, G.-H. Lee, M. Sigrist, T.-S. Lin, S.-M. Peng, *Eur. J. Inorg. Chem.* **2016**, 4250–4256; i) S.-A. Hua, M.-C. Cheng, C.-h. Chen, S. M. Peng, *Eur. J. Inorg. Chem.* **2015**, 2510–2523; j) S.-A. Hua, Y.-C. Tsai, S.-M. Peng, *J. Chin. Chem. Soc.* **2014**, *61*, 9–26; k) Y. Takemura, T. Nakajima, T. Tanase, M. Usuki, H. Takenaka, E. Goto, M. Mikuriya, *Chem. Commun.* **2009**, 1664–1666; l) I. P.-C. Liu, W.-Z. Wang, S.-M. Peng, *Chem. Commun.* **2009**, 4323–4331 *and references therein*.

[8] a) M.-C. Cheng, C.-H. Cheng, P.-J. Chen, T.-S. Lin, G.-H. Lee, Y.-C. Liu, M.-H. Chiang, S.-M. Peng, *Bull. Chem. Soc. Jpn.* **2021**, *94*, 2092–2099; b) O. Rivada-Wheelaghan, S. Deolka, R. Govindarajan, E. Khaskin, R. R. Fayzullin, S. Pal, J. R. Khusnutdinova, *Chem. Commun.* **2021**, *57*, 10206–10209; c) G. L. Guillet, K. Y. Arpin, A. M. Boltin, J. B. Gordon, J. A. Rave, P. C. Hillesheim, *Inorg. Chem.* **2020**, *59*, 11238–11243; d) N. V. S. Harisomayajula, S. Makovetskyi, Y.-C. Tsai, *Chem. Eur. J.* **2019**, *25*, 8936–8954; e) N. V. S. Harisomayajula, B.-H. Wu, D.-Y. Lu, T.-S. Kuo, I.-C. Chen, Y.-C. Tsai, *Angew. Chem.* **2018**, *130*, 10073–10077, *Angew. Chem. Int. Ed.* **2018**, *57*, 9925–9929; f) R. H. Ismayilov, F. F. Valiyev, D. B. Tagiyev, Y. Song, N. V. Israfilov, W.-Z. Wang, G.-H. Lee, S.-M. Peng, B. A. Suleimanov, *Inorg. Chim.Acta* **2018**, *483*, 386–391; g) W.-Z. Wang, D. Zhao, M.-J. Zhao, H. Li, S. Liu, R. H. Ismayilov, G.-H. Lee, S.-M. Peng, *J. Mol. Struct.* **2017**, *1130*, 748–752; h) O. Rivada-Wheelaghan, S. L. Aristizábal, J. López-Serrano, R. R. Fayzullin, J. R. Khusnutdinova, *Angew. Chem.* **2017**, *129*, 16485–16489; *Angew. Chem. Int. Ed.* **2017**, *56*, 16267–16271; i) C. Krämer, S. Leingang, O. Hübner, E. Kaifer, H. Wadepohl, H.-J. Himmel, *Dalton Trans.* **2016**, *45*, 16966–16983.

[9] a) P.-J. Chen, M. Sigrist, E.-C. Horng, G.-M. Lin, G.-H. Lee, C.-h. Chen, S.-M. Peng, *Chem. Commun.* **2017**, *53*, 4673–4676; b) R. H. Ismayilov, W.-Z. Wang, G.-H. Lee, C.-Y. Yeh, S.-A. Hua, Y. Song, M.-M. Rohmer, M. Bénard, S.-M. Peng, *Angew. Chem.* **2011**, *123*, 2093–2096; *Angew. Chem. Int. Ed.* **2011**, *50*, 2045–2048.

[10] *See for example*: a) M.-C. Cheng, G.-H. Lee, T.-S. Lin, Y.-C. Liu, M.-H. Chiang, S.-M. Peng, *Dalton Trans.* **2021**, *50*, 520–534; b) M.-C. Cheng, R.-X. Huang, Y.-C. Liu, M.-H. Chiang, G.-H. Lee, Y. Song, T.-S. Lin, S.-M. Peng, *Dalton Trans.* **2020**, *49*, 7299–7303; c) C.-C. Chiu, M.-C. Cheng, S.-H. Lin, C.-W. Yan, G.-H. Lee, M.-C. Chang, T.-S. Lin, S.-M. Peng, *Dalton Trans.* **2020**, *49*, 6635–6643; d) B.-H. Wu, J.-Y. Lin, K.-Y. Ho, M.-J. Huang, S.-A. Hua, M.-C. Cheng, Y.-W. Yang, S.-M. Peng, C.-h. Chen, I–C. Chen, *J. Phys. Chem. C* **2016**, *120*, 20297–20302.

[11] *See for example*: a) R. H. Ismayilov, F. F. Valiyev, N. V. Israfilov, W.-Z. Wang, G.-H. Lee, S.-M. Peng, B. A. Suleimanov, *J. Mol. Struct.* **2020**, *1200*, 126998; b) W.-Z. Wang, S.-B. Geng, S. Liu, D. Zhao, X.-G. Jia, H.-L. Wei, R. H. Ismayilov, C.-Y. Yeh, G.-H. Lee, S.-M. Peng, *J. Mol. Struct.* **2017**, *1138*, 222–226; c) G.-M. Lin, M. Sigrist, E.-C. Horng, C.-h. Chen, C.-Y. Yeh, G.-H. Lee, S.-M. Peng, *Z. Anorg. Allg. Chem.* **2015**, *641*, 2258–2265; d) W.-Z. Wang, D. Zhao, T.-B. Tsao, R. Ismayilov, G.-H. Lee, S.-M. Peng, *Eur. J. Inorg. Chem.* **2015**, 4329–4334.

[12] a) T.-J. Liu, S.-M. Peng, B.-Y. Jin, *New J. Chem.* **2019**, *43*, 16089–16095; b) S.-c. Hsu, G.-M. Lin, G.-H. Lee, C.-h. Chen, S.-M. Peng, *J. Chin. Chem. Soc.* **2018**, *65*, 122–132; c) J. A. Chipman, J. F. Berry, *Inorg. Chem.* **2018**, *57*, 9354–9363; d) J. A. Chipman, J. F. Berry, *Chem. Eur. J.* **2018**, *24*, 1494–1499; e) M.-C. Cheng, S.-A. Hua, Q. Lv, M. Sigrist, G.-H. Lee, Y.-C. Liu, M.-H. Chiang, S.-M. Peng, *Dalton Trans.* **2018**, *47*, 1422–1434; f) W.-C. Chang, C.-W. Chang, M. Sigrist, S.-A. Hua, T.-J. Liu, G.-H. Lee, B.-Y. Jin, C.-h. Chen, S.-M. Peng, *Chem. Commun.* **2017**, *53*, 8886–8889; g) W.-C. Hung, M. Sigrist, S.-A. Hua, L.-C. Wu, T.-J. Liu, B.-Y. Jin, G.-H. Lee, S.-M. Peng, *Chem. Commun.* **2016**, *52*, 12380–12382; h) M.-J. Huang, S.-A. Hua, M.-D. Fu, G.-C. Huang, C. Yin, C.-H. Ko, C.-K. Kuo, C.-H. Hsu, G.-H. Lee, K.-Y. Ho, C.-H. Wang, Y.-W. Yang, I–C. Chen, S.-M. Peng, C.-h. Chen, *Chem. Eur. J.* **2014**, *20*, 4526–4531.

[13] a) C.-L. Hsieh, T.-J. Liu, Y. Song, G.-H. Lee, B.-Y. Jin, T.-S. Lin, S.-M. Peng, *Dalton Trans.* **2019**, *48*, 9912–9915; b) C.-C. Chiu, G.-H. Lee, T.-S. Lin, S.-M. Peng, *Dalton Trans.* **2019**, *48*, 8464–8477; c) Y.-C. Liu, S.-A. Hua, M.-C. Cheng, L.-C. Yu, S. Demeshko, S. Dechert, F. Meyer, G.-H. Lee, M.-H. Chiang, S.-M. Peng, *Chem. Eur. J.* **2018**, *24*, 11649–11666 *and references therein*.

[14] a) T. Tanase, K. Nakamae, Y. i Ura, T. Nakajima, *Coord. Chem. Rev.* **2022**, *466*, 214581; b) T. Tanase, Y. Fujisawa, Y. Morita, Y. Ura, T. Nakajima, *Eur. J. Inorg. Chem.* **2022**, e202200248; c) T. Tanase, K. Nakamae, Y. Kitagawa, T. Nakajima, *Chem. Eur. J.* **2021**, *27*, 12953–12958; d) T. Tanase, R. Otaki, K. Nakamae, Y. Ura, T. Nakajima, *J. Organomet. Chem.* **2020**, *925*, 121488; e) T. Nakajima, T. Tanase, *Chem. Lett.* **2020**, *49*, 386–394; f) T. Tanase, M. Tanaka, M. Hamada, Y. Morita, K. Nakamae, Y. Ura, T. Nakajima, *Chem. Eur. J.* **2019**, *25*, 8219–8224; g) T. Tanase, M. Chikanishi, K. Morita, K. Nakamae, B. Kure, T. Nakajima, *Chem. Asian J.* **2015**, *10*, 2619–2623.

[15] a) M. Dahlen, T. P. Seifert, S. Lebedkin, M. T. Gamer, M. M. Kappes, P. W. Roesky, *Chem. Commun.* **2021**, *57*, 13146–13149; b) M. Olaru, J. F. Kögel, R. Aoki, R. Sakamoto, H. Nishihara, E. Lork, S. Mebs, M. Vogt, J. Beckmann, *Chem. Eur. J.* **2020**, *26*, 275–284.

[16] *See for example*: a) K. Masai, K. Shirato, K. Yamamoto, Y. Kurashige, T. Murahashi, *Chem. Commun.* **2016**, *52*, 6427–6430; b) Y. Tatsumi, T. Murahashi, M. Okada, S. Ogoshi, H. Kurosawa, *Chem. Commun.* **2008**, 477–479; c) T. Murahashi, Y. Mino, K. Chiyoda, S. Ogoshi, H. Kurosawa, *Chem. Commun.* **2008**, 4061–4063; d) T. Murahashi, Y. Higuchi, T. Katoh, H. Kurosawa, *J. Am. Chem. Soc.* **2002**, *124*, 14288–14289; e) T. Murahashi, E. Mochizuki, Y. Kai, H. Kurosawa, *J. Am. Chem. Soc.* **1999**, *121*, 10660–10661.

[17] M. Yamane, M. Yamashita, K. Yamamoto, T. Murahashi, *Phys. Chem. Chem. Phys.* **2018**, *20*, 4287–4296.

[18] S. Horiuchi, Y. Tachibana, M. Yamashita, K. Yamamoto, K. Masai, K. Takase, T. Matsutani, S. Kawamata, Y. Kurashige, T. Yanai, T. Murahashi, *Nat. Commun.* **2015**, *6*, 6742.

[19] a) M. Yamashita, S. Horiuchi, K. Yamamoto, T. Murahashi, *Dalton Trans.* **2019**, *48*, 13149–13153; b) T. Murahashi, K. Shirato, A. Fukushima, K. Takase, T. Suenobu, S. Fukuzumi, S. Ogoshi, H. Kurosawa, *Nat. Chem.* **2012**, *4*, 52–58.
[20] M. Yamashita, Y. Kawasumi, Y. Tachibana, S. Horiuchi, K. Yamamoto, T. Murahashi, *Chem. Eur. J.* **2019**, *25*, 1212–1216.
[21] a) T. Tanase, K. Nakamae, H. Miyano, Y. Ura, Y. Kitagawa, S. Yada, T. Yoshimura, T. Nakajima, *Chem. Eur. J.* **2021**, *27*, 12078–12103; b) T. Tanase, K. Nakamae, S. Hayashi, A. Okue, R. Otaki, T. Nishida, Y. Ura, Y. Kitagawa, T. Nakajima, *Inorg. Chem.* **2021**, *60*, 3259–3273; c) T. Tanase, K. Morita, R. Otaki, K. Yamamoto, Y. Kaneko, K. Nakamae, B. Kure, T. Nakajima, *Chem. Eur. J.* **2017**, *23*, 524–528; d) K. Nakamae, Y. Takemura, B. Kure, T. Nakajima, Y. Kitagawa, T. Tanase, *Angew. Chem.* **2015**, *127*, 1030–1035; *Angew. Chem. Int. Ed.* **2015**, *54*, 1016–1021; e) T. Tanase, S. Hatada, S. Noda, H. Takenaka, K. Nakamae, B. Kure, T. Nakajima, *Inorg. Chem.* **2015**, *54*, 8298–8309.
[22] E. S. Smirnova, J. M. Muñoz Molina, A. Johnson, N. A. G. Bandeira, C. Bo, A. M. Echavarren, *Angew. Chem.* **2016**, *128*, 7613–7617; *Angew. Chem. Int. Ed.* **2016**, *55*, 7487–7491.
[23] T. Tanase, K. Nakamae, H. Miyano, Y. Fujisawa, Y. Ura, T. Nakajima, *Chem. Commun.* **2021**, *57*, 11264–11267.
[24] J. M. López-de-Luzuriaga, M. Monge, S. Moreno, M. E. Olmos, M. Rodríguez-Castillo, *Angew. Chem.* **2021**, *133*, 650–654; *Angew. Chem. Int. Ed.* **2021**, *60*, 640–644.
[25] K. Uemura, *Dalton Trans.* **2017**, *46*, 5474–5492.
[26] [{Pt_2}···{Rh_2}···{Pt_2}]: a) K. Uemura, Y. Sugiyama, *J. Mol. Struct.* **2022**, *1250*, 131694; [{Rh_2}···{Pt_2}···{Rh_2}]:; b) K. Uemura, E. Yasuda, Y. Sugiyama, *ACS Omega* **2021**, *6*, 18487–18503; [{PtMPt}···{PtMPt}] (M = Mn, Fe, Co, Ni, Cu):; c) A. Takamori, K. Uemura, *Inorg. Chem.* **2022**, *61*, 5762–5778.
[27] [Rh_2}···[PtMPt]}$_\infty$: a) K. Uemura, Y. Aoki, A. Takamori, *Dalton Trans.* **2022**, *51*, 946–957 (M = Mn); b) K. Uemura, R. Miyake, *Inorg. Chem.* **2020**, *59*, 1692–1701 (M = Co); c) K. Uemura, D. Ito, J. Pirillo, Y. Hijikata, A. Saeki, *ACS Omega* **2020**, *5*, 30502–30518 (M = Pd).
[28] C. Tejel, M. A. Ciriano, L. A. Oro, *Chem. Eur. J.* **1999**, *5*, 1131–1135.
[29] a) M. Yoshida, N. Yashiro, H. Shitama, A. Kobayashi, M. Kato, *Chem. Eur. J.* **2016**, *22*, 491–495; b) E. Goto, R. A. Begum, C. Ueno, A. Hosokawa, C. Yamamoto, K. Nakamae, B. Kure, T. Nakajima, T. Kajiwara, T. Tanase, *Organometallics* **2014**, *33*, 1893–1904; c) M. Majumdar, J. K. Bera, in *Transition-metal based linear chain compounds*, (Eds: A. S. A. E. Aziz, C. E. Carraher Jr, C. U. Pittman Jr, M. Zeldin), Macromolecules Containing Metal and Metal-Like Elements, Wiley, New Jersey, **2009**, Vol. 9, pp. 181–253 *and references therein.*
[30] a) M. P. Del Río, J. A. López, M. A. Ciriano, C. Tejel, *Chem. Eur. J.* **2013**, *19*, 4707–4711; b) C. Tejel, M. A. Ciriano, B. E. Villarroya, R. Gelpi, J. A. López, F. J. Lahoz, L. A. Oro, *Angew. Chem.* **2001**, *113*, 4208–4210; *Angew. Chem. Int. Ed.* **2001**, *40*, 4084–4086; c) C. Tejel, M. A. Ciriano, J. A. López, F. J. Lahoz, L. A. Oro, *Angew. Chem.* **1998**, *110*, 1647–1650; *Angew. Chem. Int. Ed.* **1998**, *37*, 1542–1545; d) M. A. Ciriano, S. Sebastian, L. A. Oro, A. Tiripicchio, M. T. Camellini, F. J. Lahoz, *Angew. Chem.* **1988**, *100*, 406–407; *Angew. Chem. Int. Ed.* **1988**, *27*, 402–403.
[31] C. Tejel, M. A. Ciriano, B. E. Villarroya, J. A. López, F. J. Lahoz, L. A. Oro, *Angew. Chem.* **2003**, *115*, 547–550; *Angew. Chem. Int. Ed.* **2003**, *42*, 529–532.
[32] J. F. Berry, F. A. Cotton, C. A. Murillo, *Dalton Trans.* **2003**, 3015–3021.
[33] F. A. Cotton, H. Chao, Z. Li, C. A. Murillo, Q. Wang, *J. Organomet. Chem.* **2008**, *693*, 1412–1419.
[34] a) M. Spivak, V. Arcisauskaite, X. López, J. E. McGrady, C. de Graaf, *Dalton Trans.* **2017**, *46*, 6202–6211; b) J. F. Berry, F. A. Cotton, T. Lu, C. A. Murillo, B. K. Roberts, X. Wang, *J. Am. Chem. Soc.* **2004**, *126*, 7082–7096.
[35] A. Srinivasan, X. Wang, R. Clérac, M. Rouzières, L. R. Falvello, J, E. McGrady, E. A. Hillard, *Dalton Trans.* **2018**, *47*, 16798–16806.
[36] M. Yoshida, H, Shitama, W. M. C. Sameera, A. Kobayashi, M. Kato, *Chem. Eur. J.* **2019**, *25*, 7669–7678.
[37] K.-N. Shih, M.-J. Huang, H.-C. Lu, M.-D. Fu, C.-K. Kuo, G.-C. Huang, G.-H. Lee, C.-h. Chen, S.-M. Peng, *Chem. Commun.* **2010**, *46*, 1338–1340.
[38] M. Nippe, Y. Turov, J. F. Berry, *Inorg. Chem.* **2011**, *50*, 10592–10599.
[39] L. Dahlenburg, R. Menzel, F. W. Heinemann, *Acta Crystallogr., Sect. E: Struct. Rep. Online* **2007**, *63*, m2769–m2770.
[40] M. Lanfranchi, A. Tiripicchio, G. Dolcetti, M. Ghedini *Transition Met. Chem.* **1980**, *5*, 21–25.
[41] F. A. Cotton, C. Lin, C. A. Murillo, *Inorg. Chem.* **2000**, *39*, 4574–4578.
[42] Date of search: 09–12-2022. Version: 2022.3.0. C. R. Groom, I. J. Bruno, M. P. Lightfoot, S. C. Ward, *Acta Cryst.* **2016**, *B72*, 171–179.
[43] For complexes featuring the 'Cl–Ir–Ir' moiety with a Cl–Ir bond distance longer than 2.524 Å see: a) T. S. Teets, T. R. Cook, B. D. McCarthy, D. G. Nocera, *Inorg. Chem.* **2011**, *50*, 5223–5233 (2.533 Å); b) C. Tejel, M. A. Ciriano, J. A. Lopez, F. J. Lahoz, L. A. Oro *Organometallics* **1998**, *17*, 1449–1951 (2.532 Å); c) A. L. Balch, L. A. Fossett, R. R. Guimerans, M. M. Olmstead, P. E. Reedy Jr, *Inorg. Chem.* **1986**, *25*, 1397–1404 (2.599 Å); d) B. R. Sutherland, M. Cowie, *Inorg. Chem.* **1984**, *23*, 2324–2331 (2.557 Å).
[44] For complexes featuring the 'Br–Ir–Ir' moiety with a Br–Ir bond distance longer than 2.6788 Å see: A. S. Veige, T. G. Gray, D. G. Nocera, *Inorg. Chem.* **2005**, *44*, 17–26 (2.691 Å).
[45] For complexes featuring the 'I–Ir–Ir' moiety with an I–Ir bond distance longer than 2.843 Å, see references 30c (2.891 Å), 30d (2.892 Å), and 31 (2.857(2) Å).
[46] The longest NCS–Ir bond distance was reported in the tetranuclear anion $[Ir_4(CO)_{11}(SCN)]^-$ (2.454 Å, shorter than here): M. P. Brown, D. Burns, M. M. Harding, S. Maginn, A. K. Smith, *Inorg. Chim. Acta* **1989**, *162*, 287–289.
[47] K. Fagnou, M. Lautens, *Angew. Chem* **2002**, *114*, 26–49; *Angew. Chem. Int. Ed.* **2002**, *41*, 26–47.
[48] G. M. Sheldrick, SADABS, Area Detector Absorption Correction Program, Bruker AXS, Madison, WI (USA), **1997**.
[49] C. Giacovazzo, SIR-97 Program for Crystal Structure Solution, Inst. di Ric. per lo Sviluppo di Metodologie Cristallograpfiche, CNR, University of Bari, Italy, 1997.
[50] G. M. Sheldrick, *Acta Cryst.* **2008**, *A64*,112–122.
[51] G. M. Sheldrick, *Acta Cryst.* **2015**, *C71*, 3–8.
[52] L. J. Farrugia, *J. Appl. Crystallogr.* **2012**, *45*, 849–854.
[53] A. L. Spek, *Acta Cryst.* **2015**, *C71*, 9–18.
[54] Gaussian 09 (Revision D.01): M. J. Frisch, G. W. Trucks, H. B. Schlegel, G. E. Scuseria, M. A. Robb, J. R. Cheeseman, G. Scalmani, V. Barone, B. Mennucci, G. A. Petersson, H. Nakatsuji, M. Caricato, X. Li, H. P. Hratchian, A. F. Izmaylov, J. Bloino, G. Zheng, J. L. Sonnenberg, M. Hada, M. Ehara, K. Toyota, R. Fukuda, I. J. M. Hasegawa, T. Nakajima, Y. Honda, O. Kitao, H. Nakai, T. Vreven, J. A. Montgomery Jr, J. E. Peralta, F. Ogliaro, M. Bearpark, J. J. Heyd, E. Brothers, K. N. Kudin, V. N. Staroverov, R. Kobayashi, J. Normand, K. Raghavachari, A. Rendell, J. C. Burant, S. S. Iyengar, J. Tomasi, M. Cossi, N. Rega, J. M. Millam, M. Klene, J. E. Knox, J. B. Cross, V. Bakken, C. Adamo, J. Jaramillo, R. Gomperts, R. E. Stratmann, O. Yazyev, A. J. Austin, R. Cammi, C. Pomelli, J. W. Ochterski, R. L. Martin, K. Morokuma, V. G. Zakrzewski, G. A. Voth, P. Salvador, J. J. Dannenberg, S. Dapprich, A. D. Daniels, Ö. Farkas, J. B. Foresman, J. V. Ortiz, J. Cioslowski, D. J. Fox, Gaussian, Inc., Wallingford CT (USA), **2011**.
[55] a) C. Lee, W. Yang, R. G. Parr, *Phys. Rev. B* **1988**, *37*, 785–789; b) A. D. Becke, *J. Chem. Phys.* **1993**, *98*, 1372–1377; c) A. D. Becke, *J. Chem. Phys.* **1993**, *98*, 5648–5652; d) S. Grimme, J. Antony, S. Ehrlich, H. Krieg, *J. Chem. Phys.* **2010**, *132*, 154104.
[56] L. E. Roy, P. J. Hay, R. L. Martin, *J. Chem. Theory Comput.* **2008**, *4*, 1029–1031.
[57] A. V. Marenich, C. J. Cramer, D. G. Truhlar, *J. Phys. Chem. B* **2009**, *113*, 6378–6396.

Manuscript received: May 5, 2023
Accepted manuscript online: July 4, 2023
Version of record online: August 17, 2023